On MIMO performance enhancement with multi-sector cooperation in a measured urban environment

Tian, Ruiyuan; Wu, Bo; Lau, Buon Kiong; Medbo, Jonas

Published in:
IEEE Antennas and Wireless Propagation Letters

DOI:
10.1109/LAWP.2012.2198190

2012

Document Version:
Peer reviewed version (aka post-print)

On MIMO Performance Enhancement with Multi-sector Cooperation in a Measured Urban Environment

Ruiyuan Tian, *Student Member, IEEE,* Bo Wu, Buon Kiong Lau, *Senior Member, IEEE,* and Jonas Medbo, *Senior Member, IEEE*

***Abstract*—Capacity improvement of intrasite cooperative MIMO using all three 120°-sectors of a base station (BS) site is studied for the first time in a measured urban environment at $2.65\,\mathrm{GHz}$. The results show that the mean uplink capacity gain exceeds 40% in as much as $1/4$ of the coverage area, relative to the best single-sector link with no cooperation. In addition, a simple simulation model is developed for predicting the capacity gain from intrasite multi-sector cooperation. The model is used to unravel the respective roles of the BS antenna patterns and propagation mechanisms in determining cooperative performance.**

***Index Terms*—MIMO systems, Cooperative systems.**

I. Introduction

Multiple-input multiple-output (MIMO) technology will play a key role in providing the target data rate of up to 1 gigabit per second and high spectral efficiency in the upcoming International Mobile Telecommunication (IMT)-Advanced (or 4G) mobile communication systems. Moreover, more advanced MIMO techniques involving cooperation among antennas at different locations are being considered for further improving the system throughput, particularly in the cell edge region. In general, such a coordinated multipoint (CoMP) transmission and reception system can be implemented among several base station (BS) sites ("intersite") or within several sectors of a single BS site ("intrasite"). This Letter investigates for the first time single-user capacity improvement of intrasite CoMP based on measured channels involving three-sector cooperation of a single BS site in an urban macrocellular environment. In addition, to analyze the impact of BS antennas and specific propagation mechanisms on the measured capacity gain, a simple simulation model is developed based on a "one-ring" channel model using the measured antenna patterns. The discrepancy between simulated and measured performance is then attributed to propagation mechanisms not accounted for in the model.

Manuscript received December 19, 2011; revised February xx, 2012. Current version published XXXXXXXX XX, 20xx. This work was financially supported by Vetenskapsrådet under Grant 2010-468 and VINNOVA under Grant 2009-02969.

R. Tian and B. K. Lau are with Dept. of Electrical and Information Technology, Lund University, SE-221 00 Lund, Sweden. e-mail: {Ruiyuan.Tian, Buon_Kiong.Lau}@eit.lth.se.

B. Wu was with Dept. of Electrical and Information Technology, Lund University, Sweden. He is now with Dept. of Electrical Engineering, the University of Notre Dame, IN, USA.

J. Medbo is with Ericsson Research, Ericsson AB, SE-164 80 Stockholm, Sweden.

Color versions of one or more of the figures in this paper are available online at http://ieeexplore.ieee.org.

Digital Object Identifier xx.xxxx/LAWP.20xx.XXXXXXX

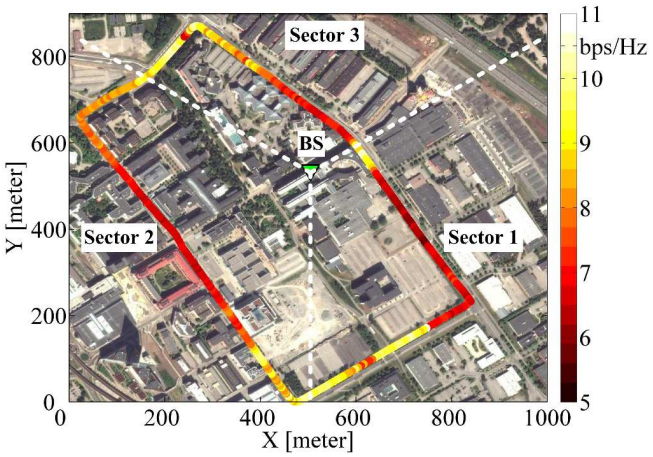

Fig. 1. Measured capacity of the uplink three-sector 6×4 cooperative MIMO channel at different locations along the drive route. The measured MIMO channels are normalized with respect to the strongest single-sector link (*i.e.*, the serving sector for the reference single-sector case) with a reference SNR of $10\,\mathrm{dB}$.

Thus far, intersite cooperation has received significantly more attention than intrasite cooperation of the CoMP system in the literature, see *e.g.*, [1]–[4]. On the other hand, intrasite CoMP requires less implementation complexity due to the antennas being co-located within a single BS site. A recent study shows that using the IMT-Advanced channel model in intrasite CoMP can lead to cooperation performance underestimation [5]. In [6], a simple CoMP precoder is found to offer promising cooperative gain using intrasite measured channels.

II. Measurements

The measurement was performed in an urban macrocellular environment at Kista, near Stockholm, Sweden. Although similar equipment and setup as that described in [4] were used, the measurement in [4] considered instead intersite CoMP systems. Therefore, here we largely focus on the unique features of the setup related to the intrasite CoMP measurement.

The considered cellular scenario is shown in Fig. 1. The BS is located on the rooftop of a building, at the height of $34\,\mathrm{m}$. It

Fig. 2. The measurement van equipped with two electric and two magnetic dipole antennas, in white and blue, respectively.

consists of three $120°$-sector antenna systems, each employing a $\pm 45°$ cross-polarized directional antenna pair and serving one of the three neighboring sectors. In our intrasite CoMP setup, the three pairs of cross-polarized antennas are assumed to cooperatively serve the entire coverage area of the three-sector BS site. The mobile station (MS) is a measurement van equipped with two electric and two magnetic dipole antennas, which have omni-directional radiation patterns and are vertical (V) and horizontal (H) polarized, respectively. The four antennas are roof-mounted and arranged as a square array with the side length of $0.3\,\mathrm{m}$. A photo of the MS antenna setup on the measurement van is given in Fig. 2.

The 6×4 channel transfer functions between all six BS antennas (in the three cooperating sectors) and four MS antennas were measured coherently using a channel sounder developed by Ericsson [4]. Relevant parameters used in the measurement setup are listed in Table I. The measurement covered a frequency bandwidth of $20\,\mathrm{MHz}$ at $2.65\,\mathrm{GHz}$, with each snapshot of the 6×4 channel being recorded every $5.33\,\mathrm{ms}$. The MS was moving along a driving route with the maximum speed of $30\,\mathrm{km/hr}$. The measured locations were logged using a GPS receiver. Using this information, the measured route is plotted in Fig. 1. The measured areas include various propagation scenarios, both with and without line-of-sight (LOS) between the BS and the MS. The signal-to-noise ratio (SNR) extracted from the channel impulse response of the strongest single-sector link (*i.e.*, the serving sector) is above $20\,\mathrm{dB}$ along the entire measurement route.

III. Capacity Analysis

In the considered uplink scenario for capacity calculations, the number of transmit antennas $N_\mathrm{T} = 4$, which is the number of MS antennas. On the other hand, the number of receive antennas $N_\mathrm{R} = 2$ in the case of single-sector links, which is the number of antennas at each BS sector. If the three-sector cooperation is considered, the total number of receive antennas becomes $N_\mathrm{R} = 6$.

To calculate the capacity, the measured MIMO channels are normalized with respect to the strongest single-sector link, *i.e.*, the serving sector. This is obtained by the following expression

$$\widetilde{\mathbf{H}}^l[f] = \mathbf{H}^l[f]/\sqrt{P_{\max}}, \tag{1}$$

TABLE I
Setup of the intrasite CoMP measurement

Parameter	Value
BS sectors	Three $120°$-sectors
BS antenna at each sector	$\pm 45°$ cross-polarized pair
MS antenna	Two V- and two H-polarized
Center frequency	$2.65\,\mathrm{GHz}$
Bandwidth	$20\,\mathrm{MHz}$
Frequency bins	162
Sampling time interval	$5.33\,\mathrm{ms}$

where $l = \{1, 2, 3\}$, and $\mathbf{H}^l[f]$ denote the measured 2×4 channel matrices of the l-th single-sector links at frequency f. The term $P_{\max}$ represents the average power of the strongest single-sector link, obtained as

$$P_{\max} = \max_l\{P^l\} = \max_l \left\{ \frac{1}{N_\mathrm{F} N_\mathrm{R} N_\mathrm{T}} \sum_{f=1}^{N_\mathrm{F}} ||\mathbf{H}^l[f]||_F^2 \right\}, \tag{2}$$

where N_F denotes the number of frequency bins, and $||\cdot||_F$ represents the Frobenius norm operator. This approach is suitable for the considered scenario with multi-sector cooperation as it defines a reference level for the channel gain of the serving sector, regardless of its path loss, and retains the relative differences in the channel gains of different sectors.

The uplink channel capacity is calculated for each of the three 2×4 single-sector links using the normalized channel matrices $\widetilde{\mathbf{H}}^l[f]$. Assuming equal power allocation, the point-to-point capacity at each location is obtained as

$$C^l = \frac{1}{N_\mathrm{F}} \sum_{f=1}^{N_\mathrm{F}} \log_2 \left[\det \left(\mathbf{I}_{N_\mathrm{R}} + \frac{\rho}{N_\mathrm{T}} \widetilde{\mathbf{H}}^l[f] \widetilde{\mathbf{H}}^l[f]^H \right) \right], \tag{3}$$

where $\mathbf{I}_{N_\mathrm{R}}$ is the $N_\mathrm{R} \times N_\mathrm{R}$ identity matrix, $\det\{\cdot\}$ is the determinant operator, $\{\cdot\}^H$ is the conjugate transpose operator, and ρ denotes the reference SNR. Here, $\rho = 10\,\mathrm{dB}$ is assumed for the single-sector link of the serving sector. For the three-sector cooperation, the 6×4 channel matrix $\widetilde{\mathbf{H}}[f]$ is obtained as

$$\widetilde{\mathbf{H}}[f] = \begin{bmatrix} \widetilde{\mathbf{H}}^1[f] \\ \widetilde{\mathbf{H}}^2[f] \\ \widetilde{\mathbf{H}}^3[f] \end{bmatrix}. \tag{4}$$

Using $\widetilde{\mathbf{H}}[f]$ in (3), the capacity C_coop of the 6×4 cooperative MIMO channel is obtained. In Fig. 1, the uplink three-sector cooperative channel capacity is illustrated along the measurement route. As can be seen, the highest cooperative capacity can be found near the edges between two neighboring sectors. This is mainly because the link power imbalance between any two neighboring sectors is the lowest in the sector edge region, which facilitates more balanced MIMO subchannels and hence larger channel capacity. In the given setup, the three-sector cooperative MIMO channel can support up to four spatial subchannels in this scenario, which corresponds to the effective cooperation of the two antenna pairs in the two neighboring sectors. The contribution of the third sector in the BS site to either spatial subchannels or capacity is negligible as the directional radiation patterns of

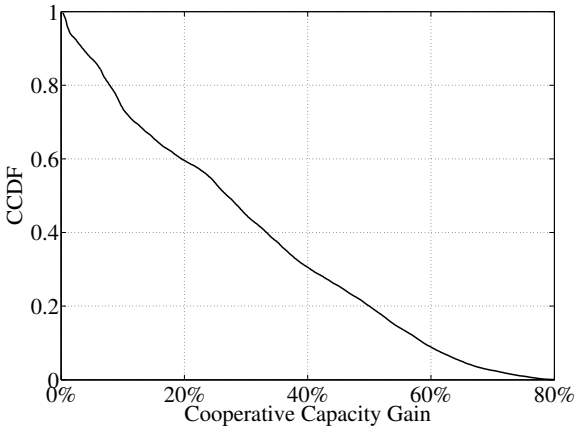

Fig. 3. The CCDF of the measured cooperative capacity gain with three-sector cooperation.

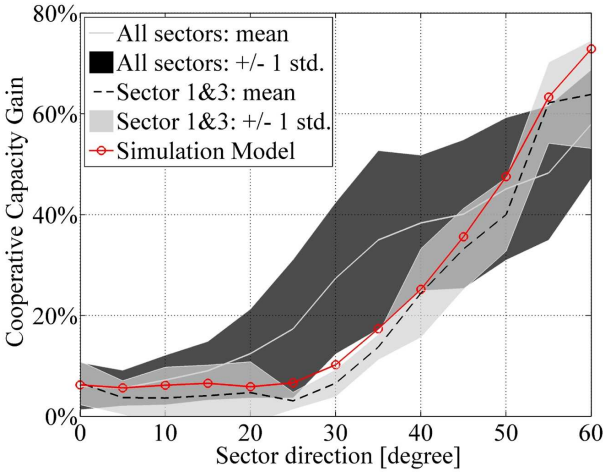

Fig. 4. Comparison between the modeled and the measured cooperative capacity gains with three-sector cooperation along the sector direction, where 0° and 60° denote the sector center and the sector edge, respectively. Both mean and standard deviation (std.) of the measured results are shown.

its antenna pair are pointing mainly in the opposite direction at that point. On the contrary, the cooperative capacity is the lowest at the center of each serving sector. This is because only two spatial subchannels can be supported due to the large power imbalance between the serving sector link and those of the neighboring sectors.

To further highlight the benefit of sector cooperation, the capacity gain is denoted as the percentage of improvement for the capacity with three-sector cooperation with respect to the highest single-sector capacity, *i.e.*,

$$\frac{C_{\text{coop}} - \max\left\{C^l\right\}}{\max\left\{C^l\right\}}, l = 1, 2, 3. \tag{5}$$

The complementary cumulative distribution function (CCDF) of the cooperative capacity gain is shown in Fig. 3. At the 50% probability level, the capacity gain is less than 30%. This is because significant cooperative gain arises mainly at the sector edges. In Fig. 4, the cooperative capacity gain is shown with respect to the sector direction, where 0° and 60° denote the sector center and the sector edge, respectively. The results from all three sectors (each with right and left halves) are merged and the statistics are calculated over 5° steps. If the sector edge region is defined as between 45° and 60°, representing 1/4 of the sector coverage, capacity gains of over 40% is attained. Moreover, since the MS route as shown in Fig. 1 is approximately uniformly distributed among all three sectors, it can be verified in Fig. 3 that up to 1/4 of the measured points have capacity gains of over 40%. This result highlights the effectiveness of the intrasite cooperation to significantly improve the capacity performance at the sector edge, where it is most needed.

IV. Modeling of Cooperative Gain

In the above capacity analysis, it is observed that cooperative capacity gain strongly depends on the direction of the MS within a given BS sector. In order to unravel the respective roles of the directional radiation patterns of the antenna pairs at the BS site and the propagation mechanisms of the considered environment, a simulation model is formulated based on the "one-ring" (single-bounce) channel assumption. The "one-ring" model is a suitable approximation for propagation environments where the BS antennas are elevated, whereas the MS antennas are surrounded by many local scatterers [7]. In our "one-ring" model, the angular spread as seen from each BS sector is assumed to be small enough so that the channel gains of all multi-paths can be approximately represented by the radiation pattern gains of the sector antenna pair in the azimuth direction ϕ of the MS. Thus, the simulated 2×4 single-sector channel is obtained as

$$\widehat{\mathbf{H}}^l(\phi) = \mathbf{H}_{\text{w}} \circ \mathbf{G}^l(\phi), l = \{1, 2, 3\}. \tag{6}$$

In the above expression, the simulated channel of the l-th sector $\widehat{\mathbf{H}}^l(\phi)$ is the Hadamard product of the independent and identically distributed (IID) Rayleigh channel matrix $\mathbf{H}_{\text{w}}$ and an antenna gain induced weighting factor of the corresponding l-th BS sector $\mathbf{G}^l(\phi)$. The simulated scenario using $\mathbf{H}_{\text{w}}$ assumes a rich multi-path scattering environment, which is mostly the case for the measured MS route. The matrix $\mathbf{G}^l(\phi)$ introduces to the MIMO channel matrix relative channel gains that are obtained from the amplitudes of the sector antennas' directional radiation patterns, which vary for different sectors and polarizations for a given MS direction ϕ.

In this work, only the azimuth antenna pattern is considered, since the MS is generally far away from the BS site and the tilt angle is neglected. Because the MS antennas are omni-directional in azimuth, only their polarization has impact on the model. In turn, the matrix $\mathbf{G}^l(\phi)$ is formed as

$$\mathbf{G}^l(\phi) = \begin{bmatrix} G^l_{\text{V}+}(\phi) & G^l_{\text{H}+}(\phi) & G^l_{\text{V}+}(\phi) & G^l_{\text{H}+}(\phi) \\ G^l_{\text{V}-}(\phi) & G^l_{\text{H}-}(\phi) & G^l_{\text{V}-}(\phi) & G^l_{\text{H}-}(\phi) \end{bmatrix}, \tag{7}$$

where $G^l_{\text{V}+}(\phi)$, $G^l_{\text{V}-}(\phi)$, $G^l_{\text{H}+}(\phi)$ and $G^l_{\text{H}-}(\phi)$ are the amplitudes of the V/H-polarized radiation patterns of the $\pm 45^\circ$ BS antennas for the l-th sector, respectively. Here we assume that the MS antennas 1 and 3 are V-polarized and antennas 2 and 4 are H-polarized. Since identical antennas are used

at all sectors, the corresponding $\mathbf{G}^l(\phi)$ for all sectors of $l = \{1, 2, 3\}$ are obtained by rotating the measured radiation patterns according to the respective bearing angles of the sectors. Finally, the 6×4 three-sector cooperative channel $\widehat{\mathbf{H}}(\phi)$ is formed by stacking the three 2×4 single-sector channels $\widehat{\mathbf{H}}^l(\phi)$ as in (4).

V. Modeling Accuracy and Insights

The single-sector capacity and cooperative capacity from the simulation model are computed for each MS direction ϕ using $\widehat{\mathbf{H}}^l(\phi)$ and $\widehat{\mathbf{H}}(\phi)$ in (3), respectively, and the capacity gain is obtained according to (5). The results are superimposed in Fig. 4. As can be observed, the simulated capacity is mostly within one standard deviation (std.) of the measured mean capacity, indicating fairly good agreement. Nevertheless, the model slightly underestimates the measured mean capacity in the transition region from the sector center to the sector edge between 15° and 45°, whereas overestimation occurs in the sector edge region between 45° to 60°. The discrepancy between the simulation and the measurement is mainly attributed to propagation mechanisms that are not accounted for in the "one-ring" channel model.

Further analysis of this result provides the following insights: 1) The underestimation is due to heavy shadowing by buildings that occurs in the serving sector link in regions between Sectors 2 and 3, which results in more balanced links from different sectors than predicted; 2) The overestimation is the result of the LOS occurrence along the route between Sectors 1 and 2, where the dominant LOS path increases the correlation in the links between different sectors and decreases the cooperative capacity. As a further confirmation, if only the region of Sectors 1 and 3 is considered, it is shown in Fig. 4 that the model can accurately track the measured results. This is further confirmed in Fig. 1 where significant cooperative capacity is attained in the angular region at the sector edge between Sectors 1 and 3.

VI. Conclusions

In this study, intrasite multi-sector cooperation has been shown to deliver significant capacity improvement in the sector edge regions of a measured urban environment. A simple simulation model is developed to gain valuable insights into the factors contributing to the achieved capacity gain. As a result, for $1/4$ of the coverage area served by a single BS site, over 40% capacity improvement is achieved with the three-sector cooperation. As future work, multi-sector cooperation will be studied for the multi-user case.

Acknowledgment

The authors would like to acknowledge Ms. Mona Hashemi and Mr. Henrik Asplund of Ericsson Research, Kista, Sweden, for providing information on the measurement setup. They also thank anonymous reviewers for their valuable comments.

References

[1] M. Alatossava, A. Taparugssanagorn, V.-M. Holappa, and J. Ylitalo, "Measurement based capacity of distributed MIMO antenna system in urban microcellular environment at 5.25 GHz," in *Proc. IEEE Veh. Technol. Conf. (VTC)*, Singapore, May 2008, pp. 430 – 434.

[2] Z. Ni and D. Li, "Effect of fading correlation on capacity of distributed MIMO," in *Proc. IEEE Personal, Indoor and Mobile Radio Commun. (PIMRC)*, vol. 3, Barcelona, Spain, Sep. 2004, pp. 1637 – 1641.

[3] V. Jungnickel, S. Jaeckel, L. Thiele, L. Jiang, U. Kruger, A. Brylka, and C. von Helmolt, "Capacity measurements in a cooperative MIMO network," *IEEE Trans. Veh. Technol.*, vol. 58, no. 5, pp. 2392 – 2405, Jun. 2009.

[4] B. K. Lau, M. Jensen, J. Medbo, and J. Furuskog, "Single and multi-user cooperative MIMO in a measured urban macrocellular environment," *IEEE Trans. Antennas Propag.*, vol. 60, no. 2, pp. 624–632, Feb. 2012.

[5] J. Zhang, G. Liu, F. Zhang, L. Tian, N. Sheng, and P. Zhang, "Advanced international communications," *IEEE Veh. Technol. Mag.*, vol. 6, no. 2, pp. 92 – 100, Jun. 2011.

[6] V. Jungnickel *et al.*, "Coordinated multipoint trials in the downlink," in *Proc. 5th IEEE Broadband Wireless Access Workshop (BWAWS), GLOBECOM*, Honolulu, US, Dec. 2009.

[7] D.-S. Shiu, G. Foschini, M. Gans, and J. Kahn, "Fading correlation and its effect on the capacity of multielement antenna systems," *IEEE Trans. Commun.*, vol. 48, no. 3, pp. 502 – 513, Mar. 2000.